Available online at www.sciencedirect.com

SciVerse ScienceDirect

Ceramics International 38 (2012) 1801–1806

CERAMICS INTERNATIONAL

www.elsevier.com/locate/ceramint

Synthesis and microstructure of Gd_2O_3-doped HfO_2 ceramics

C.K. Roy, M. Noor-A-Alam, A.R. Choudhuri, C.V. Ramana *

Department of Mechanical Engineering, University of Texas at El Paso, El Paso, TX 79968, United States

Received 20 September 2011; received in revised form 2 October 2011; accepted 3 October 2011
Available online 6 October 2011

Abstract

The effect of Gd_2O_3-doping on the crystal structure, surface morphology and chemical composition of the Gd_2O_3–HfO_2 system is reported. Gd_2O_3–HfO_2 ceramics with variable composition were prepared by varying the Gd_2O_3 composition in the range of 0–38 mol% balanced HfO_2. X-ray diffraction (XRD) analysis indicates that the Gd_2O_3 concentration influences the crystal structure of the Gd_2O_3–HfO_2 ceramics. Pure HfO_2 and Gd_2O_3 crystallize in monoclinic and body centered cubic structure, respectively. The Gd_2O_3–HfO_2 ceramics exhibit mixed monoclinic and fluorite structure when the Gd_2O_3 concentration is varied from 4 to 12 mol%. At 20 mol% of Gd_2O_3, existence of only the fluorite phase was found. Increasing the Gd_2O_3 concentration to 38 mol% results in the formation of single-phase pyrochlore $Gd_2Hf_2O_7$ (a = 5.258 Å).

Keywords: Gd_2O_3–HfO_2 ceramics; Crystal structure; Phase transformations; Thermal barrier coatings; X-ray diffraction; Scanning electron microscopy

1. Introduction

Ceramic materials based on zirconia (ZrO_2) and hafnia (HfO_2) find wide spread applications in mechanical, aerospace and energy related applications. Coatings or thin and thick films of these ceramics are desired in a number of technological applications where protection against wear, heat and harsh environments are required. Examples include aero-engines, gas turbines, coal-based advanced power generation systems, combustion and propulsion systems, boilers, fuel cells and thermal and nuclear power plants. The most important to mention are their application as thermal barrier coatings (TBCs), which prevent the damage of the engine components that are exposed to very high temperature of the hot gases [1–9]. Widespread efforts have been directed to develop the appropriate thermal barrier coating materials for high temperature application [10–27]. TBCs allow the gas turbine to operate at higher temperature by reducing the heat transfer from hot gas to superalloy blades and thereby improving the efficiency. Yttria (Y_2O_3) stabilized zirconia (YSZ) is the current industry standard TBC due to its low thermal conductivity, phase stability at relatively high temperature, high thermal expansion coefficient compared to other ceramics and good erosion resistance [3]. However, at temperature above 1200 °C, t′-tetragonal to tetragonal and cubic then to monoclinic phase transformation occurs resulting in a volume change, which leads to the formation of crack in the coatings [4,8,10]. This limits the application of YSZ at elevated temperature. Increasing demand to improve the efficiency of the gas turbines leads to search for alternate TBCs that will allow the operating temperature to increase further.

In order to develop successful TBC, it is very important to understand the behavior of the composite ceramic materials. In this context, the present work was performed on the gadolinia (Gd_2O_3) doped HfO_2 system, where Gd_2O_3 was stabilizer. It has been reported that thermal conductivity of Gd_2O_3–ZrO_2 system is lower compared to conventional Y_2O_3 stabilized ZrO_2 [23]. Also 4 mol% Gd_2O_3 stabilized ZrO_2 sintered more slowly than similar composition of Y_2O_3–ZrO_2 system [23]. Gd_2O_3–HfO_2 system has been proved to have lower thermal conductivity compared to YSZ TBCs [6]. In addition, the temperature stability of HfO_2 is higher than that of ZrO_2. It transforms into the tetragonal form when heated to at temperatures higher than 1700 °C. Further transformation into the cubic polymorphic form having the fluorite structure takes place at 2700 °C [28,29]. Therefore, it is worth investigating the Gd_2O_3–HfO_2 ceramics. Gd_2O_3–HfO_2 ceramics with variable composition were prepared by varying the Gd_2O_3 composition in the range of 0–38 mol% balanced HfO_2. The effect of Gd_2O_3-doping on the crystal structure, surface morphology and chemical composition of the Gd_2O_3–HfO_2 system is reported in this paper.

* Corresponding author. Tel.: +1 9157478690.
E-mail address: rvchintalapalle@utep.edu (C.V. Ramana).

0272-8842/$36.00
doi:10.1016/j.ceramint.2011.10.002

2. Materials and methods

Gd_2O_3–HfO_2 ceramics were prepared using conventional solid-state chemical reaction method. The ceramics were prepared by varying the composition of Gd_2O_3 in the range of 0–38 mol%, rest balanced for HfO_2. The starting materials were Gd_2O_3 (size: ~400 mesh and purity: 99.99%) and HfO_2 (size: ~400 mesh and purity: 99.95%) powders. These powders were properly ground and mixed in a mortar. Then the mixed powder was compressed in a die and punch to make 0.25 inch diameter pellet. The pressure of compression was 100,000 psi. The pellets were sintered at 1400 °C for 24 h. The resulting targets were then used for further investigation to characterize the microstructure evolution as a function of Gd_2O_3-composition. The crystal structure of the Gd_2O_3 and HfO_2 powders and Gd_2O_3–HfO_2 ceramics were investigated using a Bruker D8 Discover X-ray diffractometer employing Cu K_α radiation of wavelength 1.5406 Å. The surface morphology of the materials was examined using Hitachi S-4800 scanning electron microscope (SEM). The elemental composition and surface mapping was investigated by electron dispersive X-ray spectroscopy (EDS) analysis.

3. Results and discussion

3.1. Crystal structure and phase analysis

XRD patterns of as-received HfO_2 and Gd_2O_3 powders at room temperature are shown in Fig. 1. It is evident (Fig. 1a) that the crystal structure of HfO_2 is monoclinic with lattice parameters $a = 5.1156$ Å, $b = 5.1722$ Å and $c = 5.2948$ Å. The most intense $(-1,1,1)$ peak appeared at $2\theta = 28.356°$, which is in agreement with the literature for monoclinic HfO_2 (JCPDS No. 74-1506). Similarly, Gd_2O_3 exhibits a body centered cubic (bcc) structure (Fig. 1b) with lattice parameter $a = 10.813$ Å. The strongest (2 2 2) peak was found at $2\theta = 28.578°$ (JCPDS No. 43-1014).

The crystal structure of the Gd_2O_3–HfO_2 ceramics showed interesting structural evolution as a function of Gd_2O_3 content. XRD patterns of the Gd_2O_3–HfO_2 ceramics are shown in Fig. 2. The formation of both monoclinic and fluorite phases is evident from the XRD curves (Fig. 2a and b) for Gd_2O_3 concentration increasing from 4 to 20 mol%, at which point there is no evidence of monoclinic phase. Gd_2O_3–HfO_2 ceramics with 20 mol% Gd_2O_3 exhibit only the fluorite phase. At 38 mol%, face centered cubic (fcc) pyrochlore $Gd_2Hf_2O_7$ ($a = 5.258$ Å, JCPDS No. 24-0425) formation occurs. With the increase of Gd_2O_3 concentration from 4 to 38 mol%, the structure is changing from both monoclinic and fluorite to single fluorite and finally to FCC pyrochlore. The expanded region of the peaks where there is a visible trend indicating the changes is shown in Fig. 2c. The monoclinic $(-1,1,1)$ and fluorite intensity ratio is plotted and shown in Fig. 3. It is obvious that the monoclinic phase is decreasing with increase of Gd_2O_3 content and at 20 mol% the phase is completely fluorite. When the Gd_2O_3 concentration is 100 mol% (pure Gd_2O_3), the crystal structure was base-centered monoclinic ($a = 14.061$ Å, $b = 3.566$ Å and $c = 8.76$ Å, JCPDS No. 43-1015) which is different from Gd_2O_3 powder pattern obtained at RT. The two phases (monoclinic + fluorite) region from 4 to 12 mol% Gd_2O_3 can be viewed as partially stabilized HfO_2 because there is not enough Gd^{3+} ions to fully stabilize the HfO_2. At 20 mol% Gd_2O_3, there are enough Gd^{3+} ions to stabilize the HfO_2 fully and thus a single fluorite structure is formed. At 38 mol%, there are more Gd^{3+} ions to form the pyrochlore composition and thereby forming fcc pyrochlore structure.

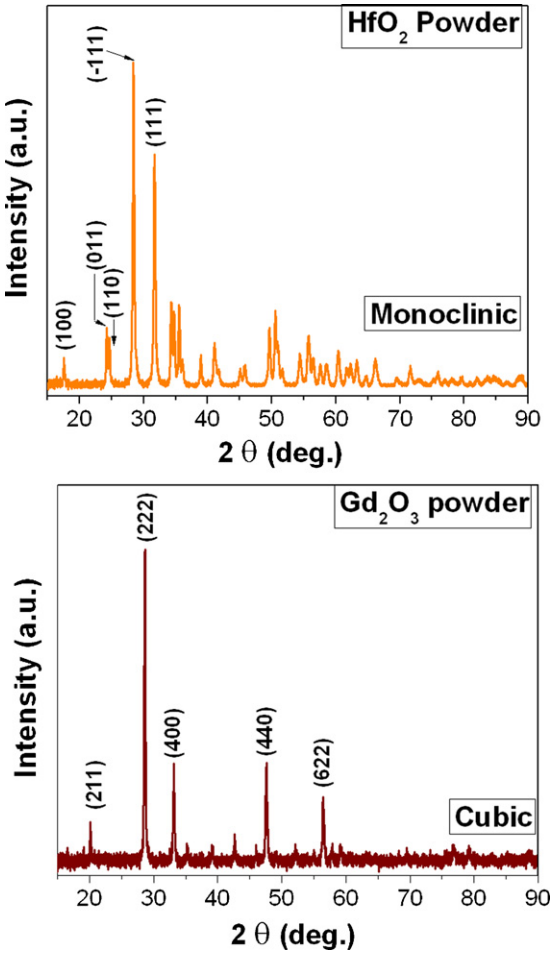

Fig. 1. XRD patterns of as received HfO_2 and Gd_2O_3 powders. The monoclinic and body centered cubic structure of HfO_2 and Gd_2O_3, respectively, are evident.

3.2. Morphology and composition

The SEM images of GSH pellets as a function of Gd_2O_3 content are shown in Fig. 4. It is evident that microstructure of the pellets changes with the Gd_2O_3 content. The morphology changes observed with progressive addition of Gd_2O_3 is believed due to the distortion as a result Gd ions interacting with the Hf ions in the ceramics. At low percentage (4%) of Gd_2O_3 the particles are smaller compared to that for higher amount of Gd_2O_3. Random void spaces are still visible all over the sample. The particles get attached together with the increase of Gd_2O_3 addition (8%). At 12% of Gd_2O_3, particles become bigger by the consumption of small particles. The void spaces decrease and pores are barely visible at this composition. The material looks very much packed at 20% of Gd_2O_3 with no visible pore. The

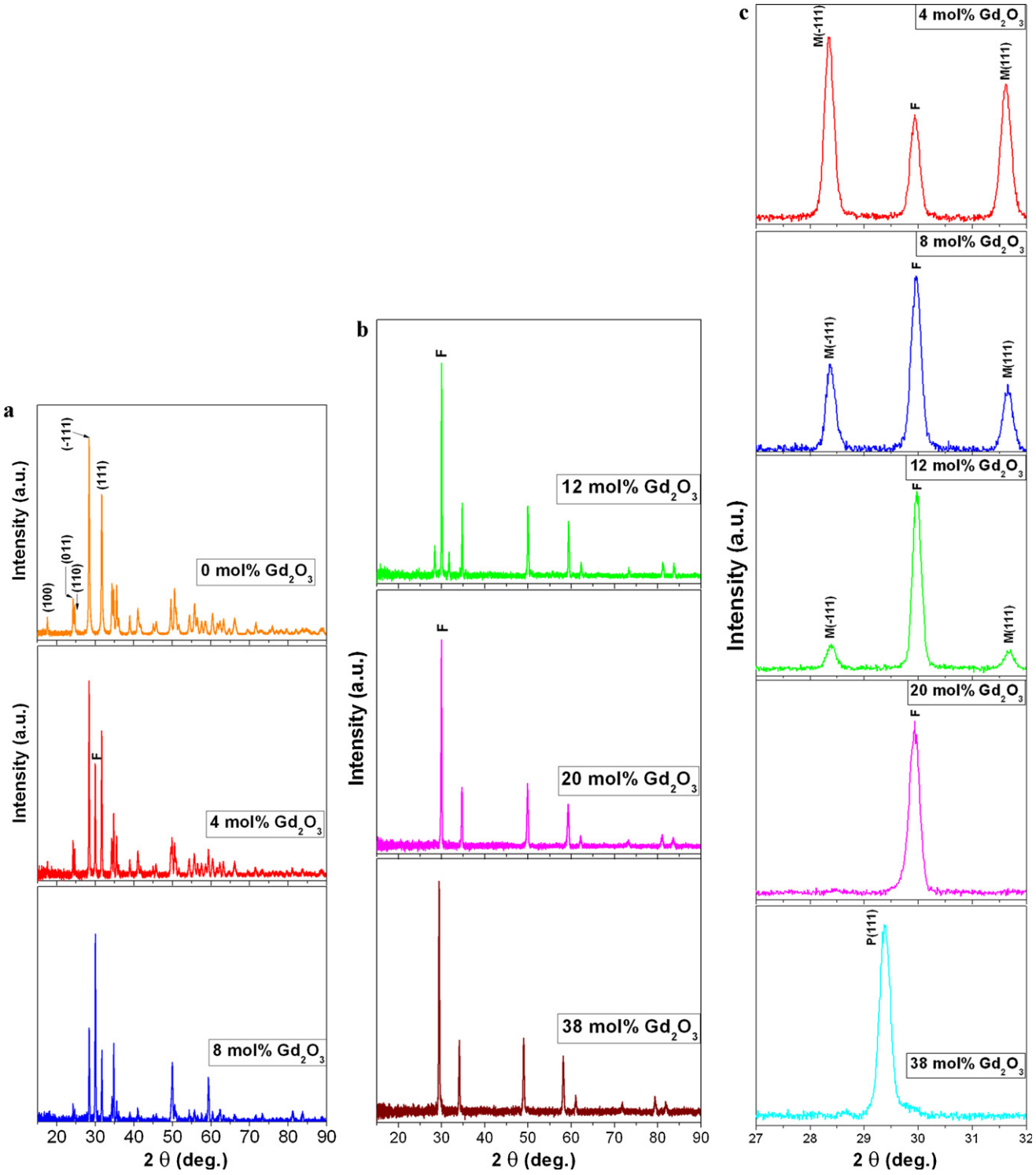

Fig. 2. (a,b) XRD patterns of the Gd_2O_3–HfO_2 ceramics. The structural evolution with increasing Gd_2O_3 content is evident from the XRD data. (c) Expanded region of the peaks indicating the phase formation in Gd_2O_3–HfO_2 ceramics.

agglomerated big domains are attached to one another without maintaining any gap in between. This change in morphology is in good agreement with the crystal structure evaluated by XRD measurement. As was evident in XRD analysis, when the structure was changing from monoclinic to fluorite the material crystallizes in one crystal structure which makes the crystal domain bigger. Because of the favorable structure the material might have smaller surface energy and get in close contact with each other making the compact surface morphology. Interestingly, the morphology is completely different at 38% of Gd_2O_3 showing round shape small particles and a lot of pores all over the sample. This is not unexpected since the material crystallizes in pyrochlore structure at 38% Gd_2O_3 because of the excess Gd^{+3} the morphology is different compared to others.

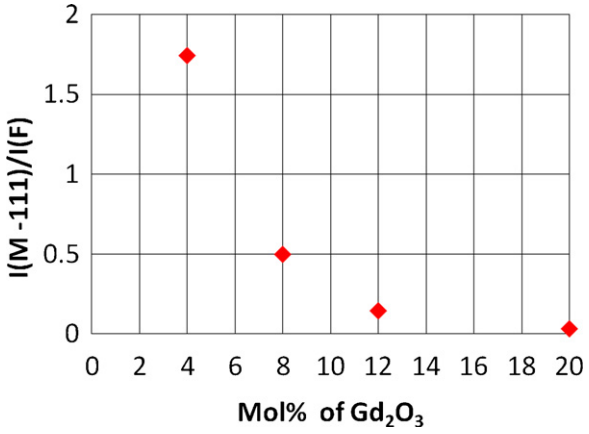

Fig. 3. Monoclinic to fluorite intensity ratio in Gd_2O_3–HfO_2 ceramics as a function of Gd_2O_3 content.

The EDS spectra of GSH pellets as a function of Gd_2O_3 concentration are presented in Fig. 5. The spectra indicate the X-rays emitted from various elements. The peaks corresponding to Gd, Hf, and O atoms present in the sample are as labeled (Fig. 5). The respective energy positions and the specific X-ray lines from various elements are also indicated in Fig. 5. The absence of any other peaks except from Gd, Hf, and O indicate the GSH pellets without any elemental impurities incorporated during chemical processing and/or handling. The peak intensity of Gd and O is increasing with the increase of Gd_2O_3 concentration as it is expected. The total Gd concentration increases from 6.85 wt% to 34.89 wt% in the GSH ceramics. The corresponding total Hf concentration decreases from 87.56 wt% to 58.12 wt% as the Gd_2O_3 content is increased from 4 to 38 mol%. The composition was very close to the starting mixing composition of the powders. This observation

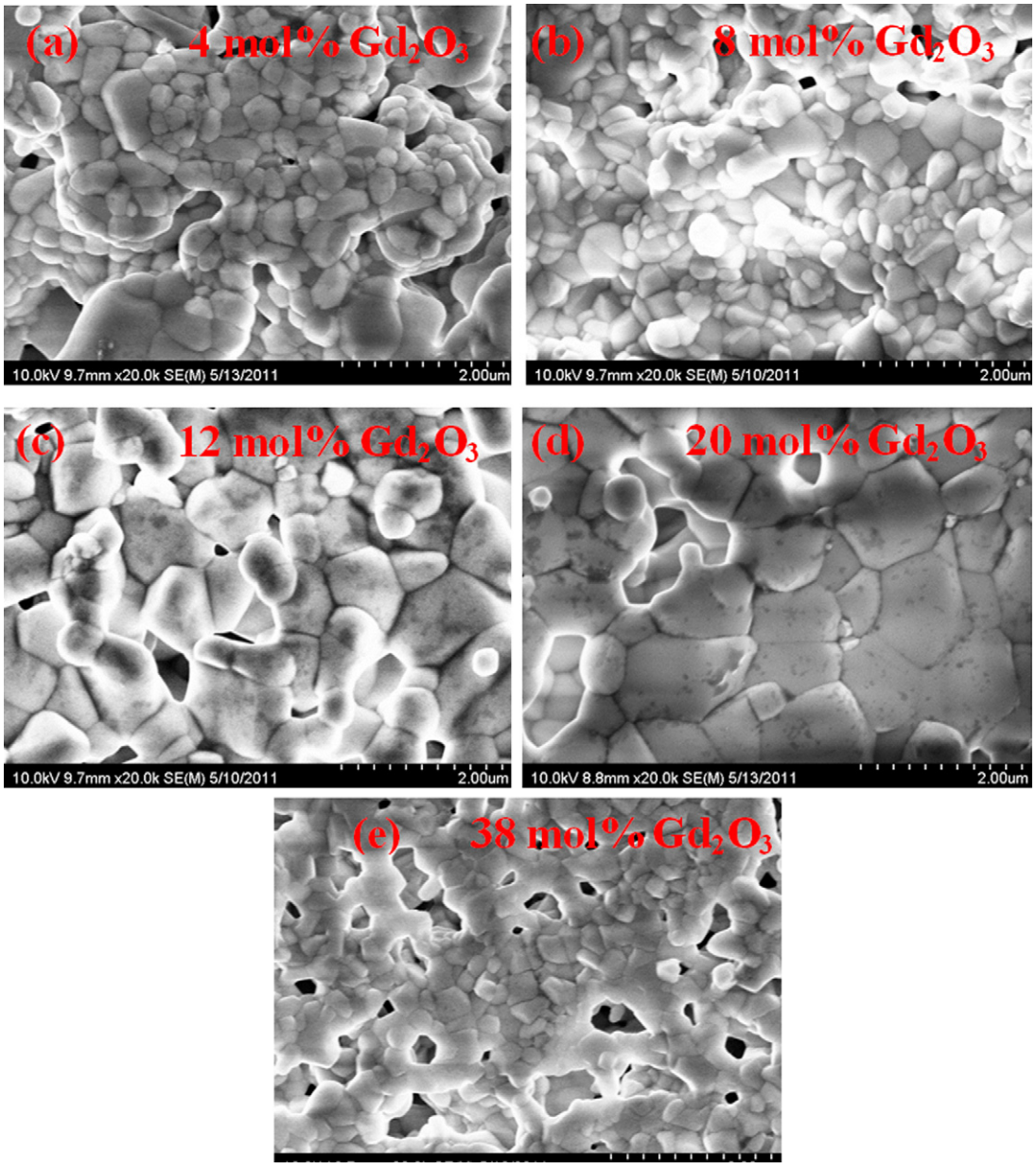

Fig. 4. SEM images of Gd_2O_3–HfO_2 ceramics as a function of Gd_2O_3 content.

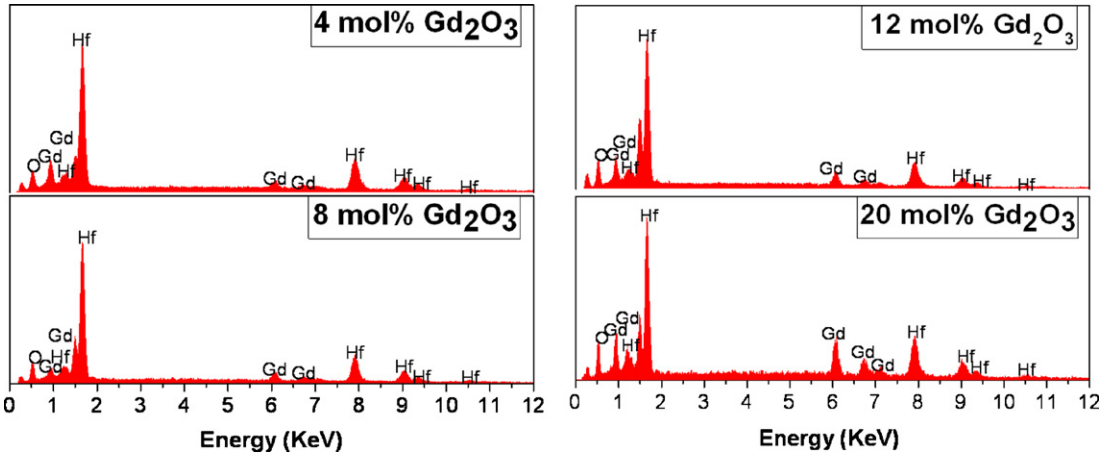

Fig. 5. EDS spectra of Gd_2O_3–HfO_2 ceramics as a function of Gd_2O_3 content.

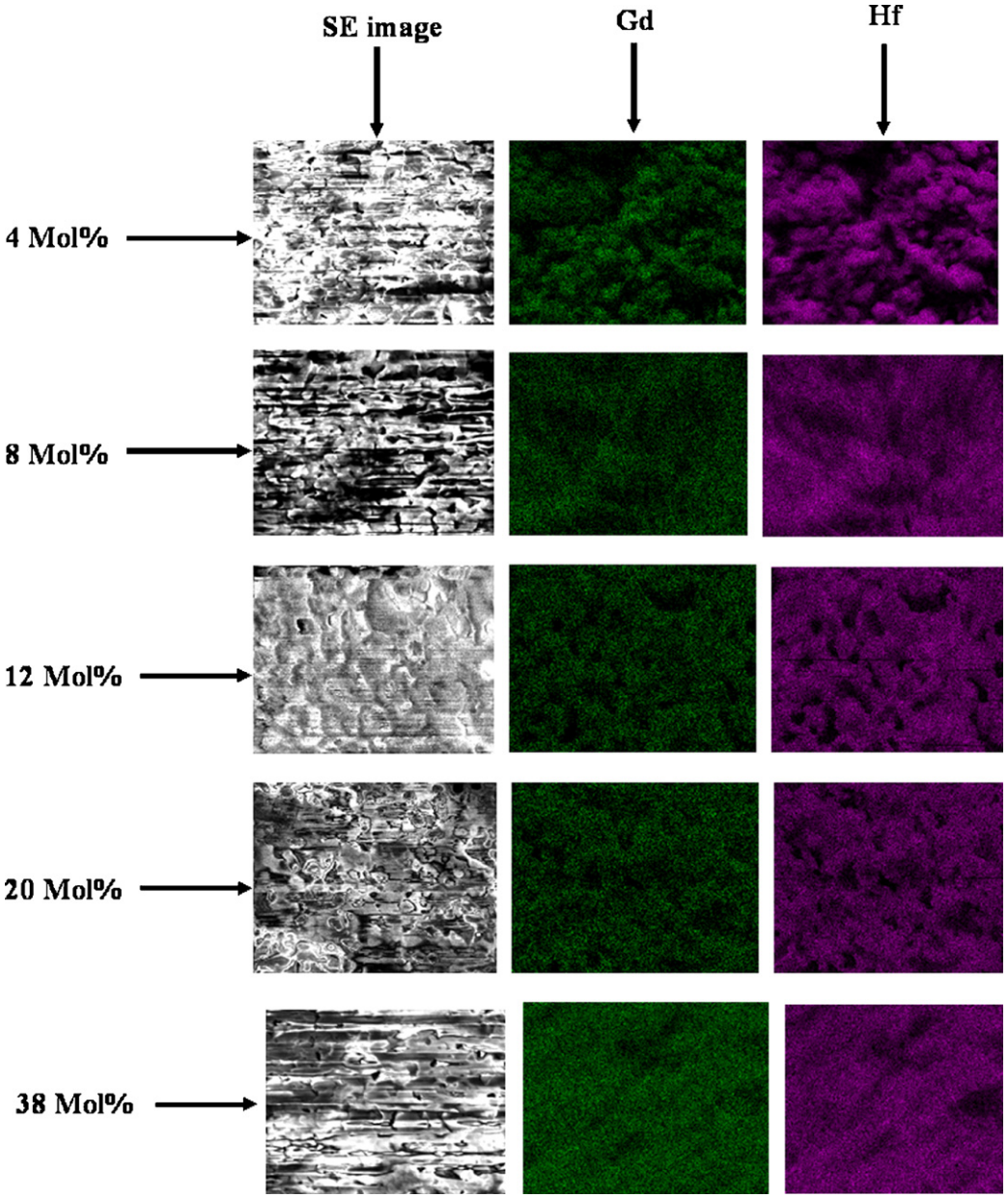

Fig. 6. Surface mapping of Gd_2O_3–HfO_2 ceramics as a function of Gd_2O_3 content. Uniform distribution of Gd, Hf and O in each of the ceramic is evident from the mapping images.

indicates that the ceramics maintain the integrity and chemical stoichiometry upon processing. Elemental mapping on across the surface of the sample (particular surface area) was performed to investigate the distribution of Gd and Hf atoms in the ceramics. Mapping images of GSH pellets, as a function of Gd_2O_3 content, are shown in Fig. 6. It is obvious from the images that the Gd concentration is increasing and Hf concentration is decreasing with the increase of Gd_2O_3 concentration and the Gd and Hf atoms are distributed evenly on this particular surface area.

4. Conclusions

The Gd_2O_3–HfO_2 ceramics were prepared by mixing and compressing the powders followed by thermal treatment at 1400 °C. XRD analyses showed that the Gd_2O_3 content influences the crystal structure and phase of the ceramics. The Gd_2O_3–HfO_2 ceramics exhibit monoclinic to a mixture of monoclinic and fluorite transition when the Gd_2O_3 concentration is varied from 0 to 12 mol%. At 20 mol% of Gd_2O_3, existence of only the fluorite phase was found. The formation of single-phase pyrochlore $Gd_2Hf_2O_7$ phase formation occurs with increasing Gd_2O_3 concentration to 38 mol%. With packing improved and single phase formation, 20 mol% of Gd_2O_3 addition seems to be optimum. The SEM imaging analysis indicates the morphological features characteristic interaction of the Gd and Hf ions. The EDS elemental composition and mapping analyses confirm the chemical composition well maintained, Gd concentration increases and homogeneous distribution characteristics of the Gd_2O_3–HfO_2 ceramics.

Acknowledgements

This material is based upon the work supported by the Department of Energy under Award Number DE-FE0000765.

References

[1] S. Bose, High Temperature Coatings, 1st ed., Butterworth-Heinemann, USA, 2007.
[2] D.D. Hass, A.J. Slifka, H.N.G. Wadley, Low thermal conductivity vapor deposited zirconia microstructures, Acta Mater. 49 (2001) 973.
[3] W. Ma, D. Mack, J. Malzbender, R. Vaben, D. Stover, Yb_2O_3 and Gd_2O_3 doped strontium zirconate for thermal barrier coatings, J. Eur. Ceram. Soc. 28 (2008) 3071.
[4] D.R. Clarke, S.R. Phillpot, Thermal barrier coating materials, Mater. Today 8 (2005) 22.
[5] K. Matsumoto, Y. Itoh, T. Kameda, EB-PVD process and thermal properties of hafnia-based thermal barrier coating, Sci. Technol. Adv. Mater. 4 (2003) 153.
[6] M.J. Maloney, Thermal Barrier Coating Systems and Materials, United States Patent, US6924040B2, August 2, 2005.
[7] R.A. Miller, Thermal barrier coatings for aircraft engines: history and directions, J. Therm. Spray Technol. 6 (1997) 35.
[8] R.A. Miller, J.L. Smialek, R.G. Garlick, Phase stability in plasma-sprayed partially stabilized Zirconia–Yttria, in: A.H. Heuer, L.W. Hobbs (Eds.), Advances in Ceramics, vol. 3, American Ceramic Society Inc., OH, 1981.
[9] X.Q. Cao, R. Vassen, D. Stoever, Ceramic materials for thermal barrier coatings, J. Eur. Ceram. Soc. 24 (2004) 1.
[10] A.G. Evans, D.R. Mumm, J.W. Hutchinson, G.H. Meier, F.S. Pettit, Mechanisms controlling the thermal barrier coatings, Prog. Mater. Sci. 46 (2001) 505.
[11] G. Soyez, J.A. Eastman, L.J. Thomson, G.R. Bai, P.M. Baldo, A.W. McCormick, R.J. DiMelfi, A.A. Elmustafa, M.F. Tambwe, D.S. Stone, Grain-size-dependent thermal conductivity of nanocrystalline yttria-stabilized zirconia films grown by metal-organic chemical vapor deposition, Appl. Phys. Lett. 77 (2000) 1155.
[12] L. Yang, Y.C. Zhou, W.G. Mao, C. Lu, Real-time acoustic emission testing based on wavelet transform for the failure process of thermal barrier coatings, Appl. Phys. Lett. 93 (2008) 231906.
[13] I. Gurrappa, A. Sambasiva, Thermal barrier coatings for enhanced efficiency of gas turbine engines, Surf. Coat. Technol. 201 (2006) 3016.
[14] N.P. Padture, M. Gell1, E.H. Jordan, thermal barrier coatings for gas-turbine engine applications, Science 296 (2002) 280.
[15] Y. Jiang, J.R. Smith, A.G. Evans, First principles assessment of metal/oxide interface adhesion, Appl. Phys. Lett. 92 (2008) 141918.
[16] D. Zhu, R.A. Miller, Sintering and creep behavior of plasma-sprayed zirconia- and hafnia-based thermal barrier coatings, Surf. Coat. Technol. 108 (1998) 114.
[17] L. Shaw, D. Goerman, R. Ren, M. Gell, The dependency of microstructure and properties of nanostructured coatings on plasma spray conditions, Surf. Coat. Technol. 130 (2000) 1.
[18] X. Cao, R. Vassen, W. Fischer, F. Tietz, W. Jungen, D. Stover, Lanthanum–cerium oxide as a thermal barrier-coating material for high-temperature applications, Adv. Mater. 15 (2003) 1438.
[19] R.S. Lima, A. Kucuk, C.C. Berndt, Evaluation of microhardness and elastic modulus of thermally sprayed nanostructured zirconia coatings, Surf. Coat. Technol. 135 (2001) 166.
[20] Z. Zhu, L. He, X. Chen, Y. Zhao, R. Mu, S. He, X. Cao, Thermal cycling behavior of $La_2Zr_2O_7$ coating with the addition of Y_2O_3 by EB-PVD, J. Alloys Compd. 508 (2010) 85.
[21] Z.-G. Liu, J.-H. Ouyang, B.H. Wang, J. Liu, Preparation and thermophysical properties of $Nd_xZr_{1-x}O_{2-x/2}$ ($x = 0.1, 0.2, 0.3, 0.4, 0.5$) ceramics, J. Alloys Compd. 466 (2008) 39.
[22] B. Saruthan, P. Francois, K. Fritcher, U. Schulz, EB-PVD processing of pyrochlore-structured $La_2Zr_2O_7$-based TBCs, Surf. Coat. Technol. 182 (2004) 175.
[23] M.N. Rahaman, J.R. Gross, R.E. Dutton, H. Wang, Phase stability, sintering, and thermal conductivity of plasma-sprayed ZrO_2–Gd_2O_3 compositions for potential thermal barrier coating applications, Acta Mater. 54 (2006) 1615.
[24] R. Vassen, F. Tietz, G. Kerkhoff, D. Stoever, New materials for advanced thermal barrier coatings, in: J. Lecomte-Beckers, F. Schuber, P.J. Ennis (Eds.), Proc. 6th Liége Conference on Materials for Advanced Power Engineering, November 1998, Universite de Liége, Belgium, ASM Thermal Spray Society, 1998, p. 1627.
[25] Ceria precipitation and phase stability in zirconia based thermal barrier coatings, A. Ohmori (Ed.), Proc. 14th International Thermal Spray Conference: Thermal spray – Current Status and Future Trends, May, 1995, Kobe, Japan, ASM International, 1995, p. 1075.
[26] X.Q. Cao, Y.F. Zhang, J.F. Zhang, X.H. Zhong, Y. Wang, H.M. Ma, Z.H. Xu, L.M. He, F. Lu, Failure of the plasma-sprayed coating of lanthanum hexaluminate, J. Eur. Ceram. Soc. 28 (2008) 1979.
[27] H. Ibegazene, S. Alperine, C. Diot, Yttira-stabilized hafnia-zirconia thermal barrier coatings: the influence of hafnia addition on TBC structure and high temperature behavior, J. Mater. Sci. 30 (1995) 938.
[28] S. Ferrari, M. Modreanu, G. Scarel, M. Fancinelli, X-ray reflectivity and spectroscopic ellipsometry as metrology tools for the characterization of interfacial layers in high-k materials, Thin Solid Films 450 (2004) 124.
[29] P. Piluso, M. Ferrier, C. Chaput, J. Claus, J.P. Bonnet, Hafnium dioxide for porous and dense high-temperature refractories (2600 °C), J. Eur. Ceram. Soc. 29 (2009) 961.